

Photocatalytic degradation of sulfonamide and its human metabolite by immobilized ZnO nanorods/TiO₂ nanoparticles

Joelma Ribeiro de Melo^{a,*}, Daiane Marques de Oliveira^a, Adriano Vinícius Scalco^a, Ana Maria Ferrari^b, Nádia Regina Camargo Fernandes^a, Marcelino Luiz Gimenes^a

^aDepartment of Chemical Engineering, State University of Maringá, Colombo Avenue 5790, 87020-260, Maringá – Brazil, emails: rmjoelma@gmail.com (J.R. Melo), daiane.marques20@gmail.com (D.M. Oliveira), scalco.adriano@gmail.com (A.V. Scalco), nrcfmachado@uem.br (N.R.C. Fernandes), marcelino.gimenes@gmail.com (M.L. Gimenes)

^bFederal University of Technology – Parana, Marcilio Dias Street 635, 86812-460, Apucarana – Brazil, email: anamferrari@utfpr.edu.br (A.M. Ferrari)

Received 27 April 2021; Accepted 10 March 2022

ABSTRACT

The heterojunction of zinc oxide (ZnO) and titanium dioxide (TiO₂) over a glass substrate was investigated. The photocatalysts were applied to sulfamethoxazole (SMX) and N-acetyl sulfamethoxazole (AcSMX) photodegradation. ZnO/TiO₂ exhibited a significant photocatalytic activity, visible light absorption and photo-stability. The best photocatalytic activity was achieved by coupling ZnO from zinc nitrate precursor with TiO₂ (N-ZT). Degradation of 49% for SMX and 32% of AcSMX were observed after 240 min of irradiation. The degradation efficiency of SMX still reached 85% and 39% for AcSMX after 12 h under irradiation. For AcSMX metabolite, an interestingly photocatalytic back-transformation to SMX was observed, indicating that this metabolite may serve as an environmental source of the sulfonamide antibiotic. The electrical energy required for SMX and AcSMX photocatalytic degradation was extremely high, although the results showed that application of ZnO/TiO₂ was efficient in reducing the toxicity of the effluent. The main toxic effect was the inhibition of root growth for *Lactuca sativa* seeds, without inhibiting seed germination. Some byproducts generated by SMX degradation were responsible for cytotoxicity against *Artemia salina*. At the same time, no toxicity were found on the treated sample after AcSMX degradation for both *Artemia salina* and *Lactuca sativa* bioindicators.

Keywords: Heterogeneous photocatalysis; Sulfamethoxazole; N-acetyl sulfamethoxazole; Semiconductor heterojunction

1. Introduction

Sulfamethoxazole (SMX) is an antibiotic drug widely used in human and veterinary medicines to prevent various bacterial infections. However, it is not completely metabolized, no matter in human or animal bodies. It can be discharged into the wastewater through its original form and as a large fraction of metabolites [1–3].

Unfortunately, sulfamethoxazole is one of the most detected sulfonamides in wastewater and is relatively

difficult to be degraded during conventional treatment processes [4–6]. Knowing that some metabolites retain biological activity and potentially retransform to the parent compound, Bonvin et al. [7] emphasized the importance of control and reduction of antibiotics and metabolites from water environments. This has become a major public concern.

Given to the wide presence in the aquatic environment, SMX antibiotic is believed to pose potential dangers to environmental ecosystems and human health even at trace levels [8–11].

* Corresponding author.

The most prominent SMX metabolite is N-acetyl sulfamethoxazole (AcSMX), which represents 50% of the excreted administered dose, given that only 14% of ingested SMX is excreted in its original form [1]. In addition, there is evidence that AcSMX may be transformed back to the parent compound during wastewater treatment [12], in water sediment tests [13] and photolytic degradation in water [7].

Therefore, it is not realistic to treat SMX and its metabolites through wastewater traditional treatment plants (WWTPs). In recent years, visible light photocatalytic technique has provided a promising and environmentally friendly solution among advanced oxidation processes (AOP) [14–16].

The solar light absorption is essential to a commercial photocatalytic process, since semiconductors often suffers from low solar energy utilization efficiency. From the reported studies, the wide band gap of semiconductor photocatalyst results in a low photocatalytic activity under visible light irradiation, such as TiO₂ and ZnO that can only utilize ultraviolet part of solar spectrum [17,18]. Thus, many researchers try to prepare narrow band gap photocatalyst matching the visible-light spectrum.

Currently, semiconductor–semiconductor heterojunctions can extend the spectral range for light absorption and enhance electron–hole separation [19]. Previous works have demonstrated that the heterojunction of TiO₂ and ZnO can result in synergic effects due to the injection of conduction band electrons from ZnO to TiO₂, decreasing the recombination rate and increasing the lifetime of the electron-hole pair [20]. Besides, their band alignment, morphology and surface defects play an important role in photocatalytic performance. Some works reported that ZnO nanorods exert a swift pathway for the transportation of photocarriers resulting in better photocatalytic activity [21–23]. As revealed in various publications, also ZnO photocorrosion could be minimized by coupling with chemically stable TiO₂ [24,25].

The most important works considering ZnO/TiO₂ photocatalyst deal with dye discoloration, reduction of hexavalent chromium, antibacterial activities and degradation of

organic pollutants [26,27]. However, it should be noted that most of the work have been conducted under UV irradiation, indicating that there is still possibility for improvement so that ZnO/TiO₂ can be efficiently used for visible light photocatalysis. TiO₂-ZnO/clay nanoarchitectures for pharmaceuticals degradation was reported and regarded as a potential visible light-promoted catalyst [28].

With this background, the objective of this study was to remove SMX and human metabolite (AcSMX) from water by photocatalytic oxidation using the ZnO/TiO₂. This study presents the effects of key parameters such as catalyst and pH, and the required energy consumption, in addition to toxicity analysis. Possible mechanisms associated with photocatalytic oxidation of SMX and AcSMX over the photocatalyst are also addressed.

2. Materials and experimental methods

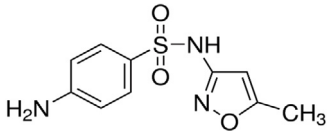
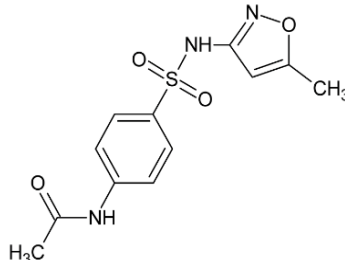
2.1. Target compounds

Sulfamethoxazole (SMX, CAS 723-46-6) and N⁴-acetyl-sulfamethoxazole (AcSMX, CAS 21312-10-7) used were of analytical grade. The characteristics of these compounds are given in Table 1. Ultrapure water with a resistivity of 18.2 MΩ cm⁻¹ was used to prepare the aqueous compound solutions.

2.2. Preparation of ZnO nanorods by solochemical process

Among the techniques known for ZnO production, the one chosen in this work was the solochemical. ZnO was prepared according to studies carried out by Wahab et al. [32] and Gusatti et al. [33]. Two different precursors were tested in alkaline solution: zinc acetate (Zn(CH₃COO)₂) or zinc nitrate (Zn(NO₃)₂). The precursor solution was prepared by dissolving the precursor in deionized water (DI) at room temperature at concentration of 0.5 M. The corresponding precursor solution was added dropwise in an alkaline solution (1.0 mol L⁻¹ NaOH) under stirring for 1 h,

Table 1
Characteristic of the commercial compounds [29–31]

Compound	Molar mass (g mol ⁻¹)	pK _{a1}	pK _{a2}	Chemical structure
Sulfamethoxazole (C ₁₀ H ₁₁ N ₃ O ₃ S)	253.27	1.85	5.6	
N-acetyl sulfamethoxazole (C ₁₂ H ₁₃ N ₃ O ₄ S)	295.3	–	5.5	

Chemical structure was obtained from ChemSketch.

at 70°C. After complete addition of the precursors to the NaOH solution, the suspension was aged for 2 h, under the same temperature and stirring conditions. The materials were then filtered, washed with DI and dried at 70°C for 12 h. The powders were denoted as ZnO-N for the material from $\text{Zn}(\text{NO}_3)_2$ and ZnO-A from $\text{Zn}(\text{CH}_3\text{COO})_2$ precursor.

2.3. Preparation of ZnO/TiO₂ thin films

Prior to film deposition, glass microscope slides (3 cm²) were first mechanically polished with silicate powder. The slides were then separately cleaned with acetone and distilled water, submitted to ultrasonic bath for 15 min and dried at room temperature. The ZnO-N/TiO₂ and ZnO-A/TiO₂ films were prepared according to Melo et al. [20]. The ZnO-N and ZnO-A powders were dissolved in water:acetic acid mixture (volume ratio 9:1) at concentration of 1.0 g L⁻¹. Subsequently, the ZnO solutions were separately added to a solution containing ethanol:titanium butoxide:acetylacetonate (volume ratio 1.0:1.0:0.5), under vigorous stirring for 2 h. A yellowish stable sol solution was obtained. ZnO-N/TiO₂ and ZnO-A/TiO₂ three-layer films (hereafter named N-ZT and A-ZT, respectively) were deposited from the corresponding sol solutions by a dip-coating technique at a withdrawal rate of 1 mm s⁻¹, followed by dehydration at 100°C for 30 min and calcination at 450°C for 90 min at a constant heating rate of 3°C min⁻¹.

2.4. Characterization techniques

Structural phase was acquired through X-ray diffraction (XRD) measurements that were performed on a Bruker-AXS D8 Advance X-ray diffractometer with Ni-filtered Cu K α radiation at a nominal power source of 40 kV \times 30 mA. Peaks observed from the diffractograms were compared with the data of PDF cards published by the International Center of Diffraction Data. The Raman spectra of the materials were acquired through a Vertex 70V FTIR (Bruker) spectrometer with external measurement accessories RAM II FT-Raman module and the RamanScope III FT-Raman microscope. Using a 532 nm-green laser (10 mW) as an excitation source, the acquisition time was 50 s, in the wavenumber range

between 50 and 800 cm⁻¹ with 10 scans. The Fourier-transform infrared spectroscopy (FTIR) were acquired by the same Vertex 70V spectrometer, in the wavenumber range between 4,000 and 400 cm⁻¹ with a resolution of 4 cm⁻¹. 15 scans were carried out during the measurements. The morphologies of ZnO powders and ZnO/TiO₂ films were observed by scanning electron microscopy (SEM, FEI Quanta 250 FEG).

The optical band gaps of the films were estimated by photoacoustic spectroscopy (PAS) by using the Tauc method [34–36]. PAS measurements were performed in an equipment consisting of a monochromatic light provided by a xenon lamp of 1,000 W (Oriel Corporation 68820), a monochromator (Oriel Instruments 77250), a high-sensitivity capacitive micro-phone (Bruel & Kjaer 2639) and a lock-in amplifier (EG&G 5110). The light beam was modulated with a mechanical modulator (Stanford Research Systems SR540). Photoacoustic spectra were obtained on modulation frequency of 21 Hz, at wavelength range between 200 and 800 nm with 10 scans. Based on the band gap energy value, it was possible to predict which region of the electromagnetic spectrum this energy was located in. Thus, the wavelength corresponding to the band gap energy of the catalysts were calculated.

In order to investigate the surface charge properties of the materials the point of zero charge (pH_{PZC}) was determined. The pH_{PZC} value were determined using the procedure as follows [37]: 25.0 mL 0.01 mol L⁻¹ NaCl solution was prepared and divided into 10 vessels. The pH of each vessel was adjusted from 2.5 to 11 by addition of H₃PO₄ and NH₄OH with suitable molarity. Thereafter, 0.20 mg of the material was added to the solutions. The mixture was shaken at 120 rpm and 25°C for 24 h. Then, the pH of each supernatant solution was measured. The final pHs vs. initial pHs were plotted to obtain pH_{PZC} . The pH_{PZC} could be determined at the point where the line of final pH was crossing the line of initial pH.

2.5. Batch experimental set-up and procedure

An Illustration of the photochemical reactor is shown in Fig. 1. The irradiation was performed in a glass batch photoreactor. A germicidal 15 W tubular UV-C lamp

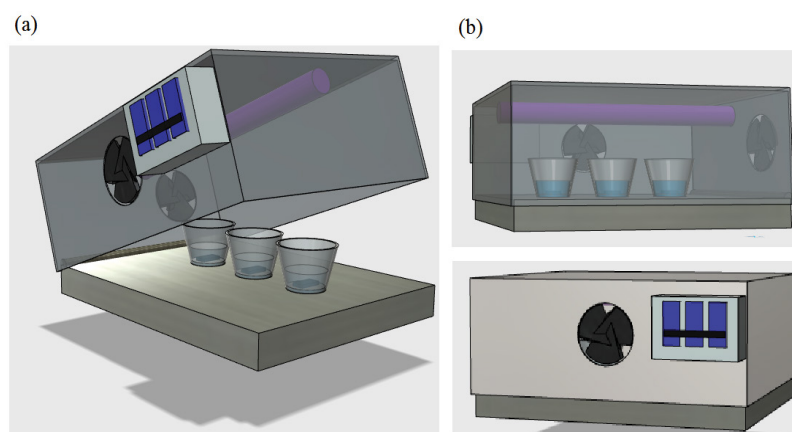


Fig. 1. Representation of the reaction unit with a view: (a) side with open lid and (b) side with closed lid.

(0.7 mW cm⁻²) or an 15 W actinic tubular visible lamp (0.47 mW cm⁻²) was placed at the top of the reaction unit, at a distance of 14 cm from the surface.

In a typical photocatalytic experiment, three vessels with 50 mL of SMX or AcSMX solution (2, 4 or 6 mg L⁻¹) were placed inside the reactor. In each vessel, two glass slides containing approximately 1.0 mg of catalyst per cm² were inserted. The tests were carried out at acidic, neuter or basic medium with pH values (pH 4.0, 7.0 and 9.0). In order to determine the best operational parameters, preliminary experiments with a solution of SMX (6 mg L⁻¹) were performed. Next, AcSMX degradation was also studied. The initial pH of solution was adjusted by adding H₃PO₄ or NH₄OH. Prior to the reaction, the solution with the photocatalyst was kept in the dark for 60 min in order to achieve adsorption-desorption equilibrium. After that, the lamp was switched on and 0.5 mL aliquots were taken at defined time intervals, during a period of 240 min. The temperature was kept at 25°C ± 2°C. The mixing of the medium was carried out by bubbling air at a flow rate of 0.50 mL s⁻¹.

2.5.1. Photolytic batch experimental procedure

Aiming to evaluate the effect of radiation on the degradation of contaminants, photolysis with UV-C and UV-Vis radiations without catalyst were studied. Emission spectra of the lamps were acquired in a VS140 linear array UV-Vis and Vis spectrometer (HORIBA). The intensity of the radiation emitted by the lamps was monitored with a radiometer (Instrutherm model MRU-201 and MRU-203).

2.6. Analytical determinations

The concentration of the compound in each sample was measured using a high-performance liquid chromatography (HPLC, Varian 920). A C₁₈ column (4.6 mm × 150 mm, 110 Å) with 5 µm particles attached to a pre-column (4 mm × 3 mm) was used. The mobile phase was a mixture of acidified water (A) with formic acid (1% v/v) and acetonitrile (B) at 70:30 ratio, in a flow rate of 1.0 mL min⁻¹. The injection sample volume was 20 µL. The detection wavelength was 270 and 254 nm for SMX and AcSMX, respectively, according to the absorption peaks (S2). All analyses were performed at 30°C. The degradation efficiency (%) was calculated by Eq. (1).

$$\text{Removal efficiency (\%)} = \frac{(C_0 - C)}{C_0} \times 100 \quad (1)$$

where C₀ is the SMX or AcSMX initial concentration, and C is the concentration at a time "t". All the experimental data were expressed in terms of arithmetic averages obtained from triplicates.

2.7. Kinetic study

Photocatalytic degradation of sulfamethoxazole and N-acetyl-sulfamethoxazole were adjusted to pseudo-first-order kinetics. The relationship between the pseudo-first-order rate constant (k_{app}) and initial concentration of compound could be described by Eq. (2):

$$r = -\frac{d[C]}{dt} \cong k_{app} \cdot C \quad (2)$$

Integration of Eq. (2) provides the pseudo-first-order rate (k_{app} min⁻¹) by equation:

$$-\ln \frac{C}{C_0} = k_{app} \cdot t \quad (3)$$

where C₀ is the initial concentration of SMX or AcSMX in mg L⁻¹, r (mg L⁻¹ min⁻¹) is the rate of surface reaction and k_{app} (min⁻¹) is the apparent kinetic constant. Therefore, k_{app} values for each initial concentration were found from the slope of straight line of ln(C/C₀) vs. reaction time plot. Finally, the half-live times (t_{1/2}) could be obtained from Eq. (4):

$$t_{1/2} = \frac{\ln 2}{k_{app}} \quad (4)$$

2.8. Electrical energy consumption (EE/O)

Among significant factors in selecting a waste-treatment technology, economics is often paramount. Electrical energy per order (EE/O) is defined as the number of kWh of electrical energy required to reduce the concentration of a pollutant by 1 order of magnitude (90%) in 1 m³ of contaminated water. The EE/O (kWh m⁻³ order⁻¹) was calculated from the following equation for pseudo-first-order kinetics [38]:

$$\frac{EE}{O} = \frac{P \cdot t \cdot 1,000}{V \cdot \log(C_0 / C)} \quad (5)$$

where P is sum of input power (kW), t is irradiation time (h), V is the volume (L) of the wastewater, C₀ is the initial concentration of target compounds and C is the final concentration of target compounds.

2.9. Toxicity assay

2.9.1. Toxicological test with *Artemia salina*

A brine shrimp (*A. salina*) assay was applied in order to perform a screening test for the lethality of the non-treated and treated effluent solutions based on the LC₅₀ criterion. Using a nutritive solution described by Garcia et al. [39], the cyst-like eggs hatched within a few hours. The most resistant nauplii were used in the toxicity assay. 2 mL of a mixture of effluent sample and nutritive solution was prepared in a 10 mL glass tube in five dilutions (15%, 35%, 50%, 75%, and 100%) of non-treated and treated effluent in triplicates, in which 10 *A. salina* nauplii were incubated at room temperature. As a control assay, 10 *A. salina* nauplii were also incubated in a pure nutritive solution. The pH was adjusted when necessary. After 24 h, the alive nauplii were counted, and lethal concentration for 50% of the organisms (LC₅₀) could be estimated.

2.9.2. Toxicological test with *Lactuca sativa*

The residual toxicity of SMX and AcSMX was also measured using *Lactuca sativa* seeds (butter lettuce) as a

producing trophic level test organism according to the method reported by Ecological Effects Test Guideline – Seed Germination/Root Elongation Toxicity Test (OPPTS 850.4200) (USEPA, 1996) [40]. Sterilized filter papers were placed in a Petri dish with 4 mL of the sample (H_2O , SMX, AcSMX and treated effluents) and then twenty *L. sativa* seeds were placed over each filter paper. The incubation was performed at a photoperiod and humidification equipped chamber during 120 at $25^\circ C \pm 2^\circ C$. The negative control was distilled water and the positive control was pure SMX or AcSMX. All the samples were tested in triplicate.

The number of seeds germinated (SG) and the root elongation (RE) were measured. Samples with more than 50% of inhibition (IC_{50}) in germination or root growth were considered potentially cytotoxic in relation to the control group. The studies were carried out without dilution, considering that the dilution would further decrease the toxicity of the samples [41].

3. Results and discussion

3.1. Catalysts characterization

Diffraction patterns of the materials are presented in Fig. 2a. The formation of a crystalline phase in immobilized

material was observed, in addition to the amorphous structure attributed to the support (glass). The diffraction peaks indicated preferential formation of TiO_2 . The main peaks at 25.3, 37.9 and 48.4 degrees corresponds to the 101, 103 and 200 planes of tetragonal anatase TiO_2 structure (ICSD card n.º 00-001-0562). Previous works have also observed the formation of anatase phase in mixed ZnO/TiO_2 catalysts [42–45]. In fact, it has been reported that ZnO/TiO_2 catalysts with small Zn content did not show diffraction peaks corresponding to ZnO [46]. However, the addition of a second component to a metal oxide can inhibit or delay the crystallization because of heterojunction [47]. The decrease on the intensity of the planes, especially the plane (101), as shown in Fig. 2b, indicates that zinc is entering the structure of the anatase phase of TiO_2 , suggesting an interaction between the two oxides [44,46,48]. By applying the Scherrer equation, the average crystallite sizes of TiO_2 , N-ZT and A-ZT were found to be 22.2, 36.4 and 24.3 nm, respectively.

Micro-Raman spectra of the TiO_2 , N-ZT and A-ZT films are shown in Fig. 2c. The peaks at 142, 196, 396, 515 and 637 cm^{-1} correspond to anatase phase of TiO_2 [49–51]. Nonetheless, the intensity decrease of some anatase peaks were observed. These signals were ascribed to the presence of wurtzite-type ZnO in the TiO_2 nanoparticle coating [52,53]. With the purpose of corroborating the formation of

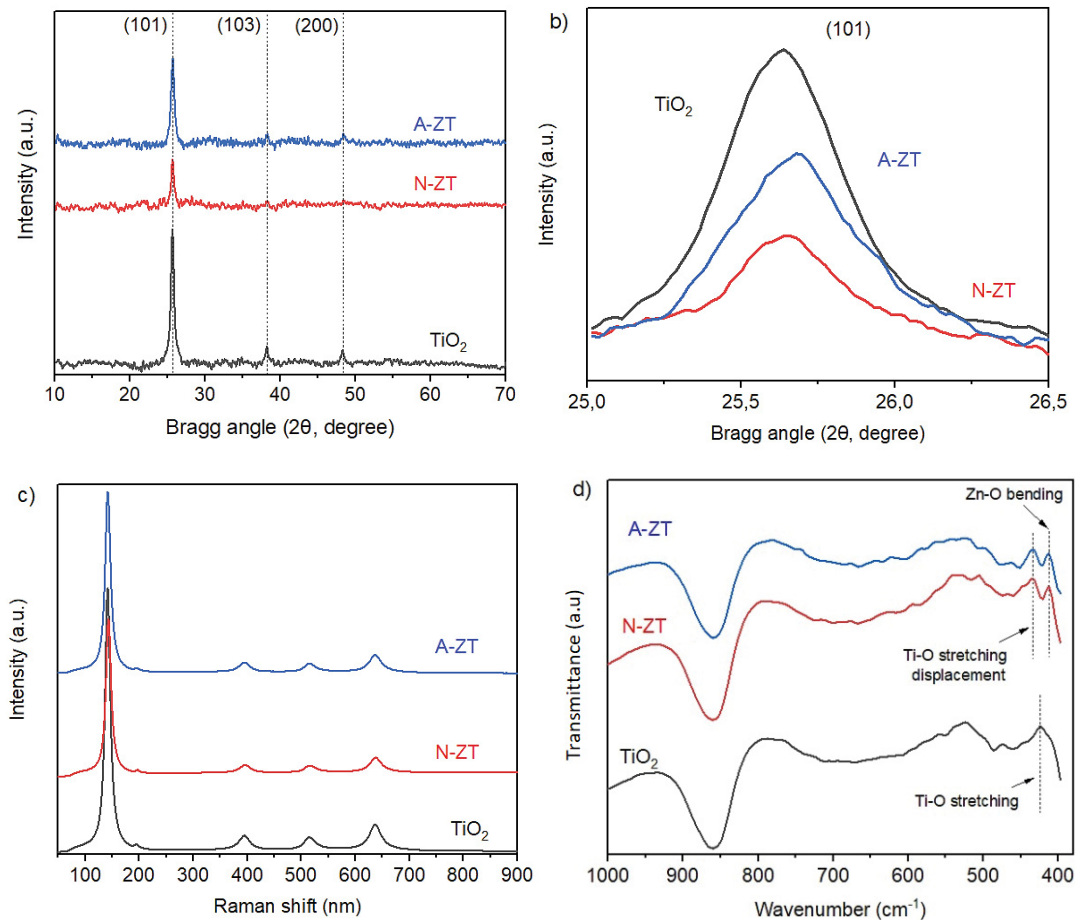


Fig. 2. (a) XRD patterns, (b) larger view of the plan [101] in the diffractogram, (c) micro-Raman spectra, and (d) FTIR spectra at 1,000–400 cm^{-1} .

TiO₂/ZnO heterostructure, FTIR measurements were performed. TiO₂, N-ZT and A-ZT films displayed four absorbance bands, representative of vibrations at 3,600; 1,690; 2,800 and 1,300 cm⁻¹ associated with O–H stretching and bending in H₂O molecules, C–H and C–O antisymmetric and symmetric stretching, respectively (Fig. 2d). The bands in the range of 400 to 1,000 cm⁻¹ provided important information about the metal-oxygen bond vibration (Ti–O or Zn–O) [54,55]. Bands with frequencies of 430, 486, 500 and 708 cm⁻¹ were associated with Ti–O stretching and Ti–O–Ti vibrations [56–58]. For photocatalysts films with ZnO addition (N-ZT and A-ZT), the absorption band at 420 cm⁻¹ can be attributed the Zn–O bending [59], which caused a displacement at 430 cm⁻¹ observed in Ti–O stretching, as shown in Fig. 2d. The broad absorption peak appearing at 800–900 cm⁻¹ is characteristic for non-reacted products.

SEM images of N-ZT and A-ZT films presented cracked surfaces (Fig. 3). The surface of a pure TiO₂ film was also analyzed for comparative purposes. Cracks appeared due to capillary pressure increase during drying stage, generating stress gradients on the surface [60,61]. The thickness of TiO₂, N-ZT and A-ZT films were found to be approximately 2.6 μm.

The optical properties of the composite films and corresponding band gap (E_g) estimated by Tauc method can be seen in Fig. 3d. The E_g values of TiO₂, N-ZT and A-ZT films were 3.02, 2.96 and 2.89 eV, respectively, indicating the extension of the photon absorption to the visible region [62]. The visible-light harvesting from this kind of material has been associated with the formation of intraband

gap energy levels in the semiconductor. For the composite films, the metal-oxide heterojunctions promote the formation of interfacial, donor or acceptor energy states mainly composed of metal-cation energy levels [63,64]. Melo et al. [20], reported that individual ZnO nanorods grown from nitrate and acetate anions also produced intraband gap energy levels to absorb low-energy photons from the visible region, with E_g values of 2.09, and 2.03 eV for N-ZT and A-ZT films, respectively, corresponding to wavelengths of 593 and 610 nm. The difference on band-gap values of N-ZT and A-ZT can be assigned to the different ZnO precursors, leading to different organizations of the electronic structure. Observing the lamp emission spectra (Fig. S1), it can be noticed that ZnO/TiO₂ catalysts can be activated by absorbing the visible light from the actinic lamp.

3.2. Photolysis

It was expected that SMX and AcSMX easily degraded under ultraviolet (UV) radiation due to its UV-Vis absorption spectra (Fig. S2). Fig. 4 shows that the degradation of SMX and AcSMX under UV-C radiation (germicidal lamp) was different from that under UV-Vis radiation (actinic lamp). Recalcitrant behavior of AcSMX was observed for both treatments. The rapid SMX degradation was mainly attributed to direct UV photodegradation [65,66]. The absorption of UV light at 254 nm leads to formation of excited state of SMX. One of main mechanisms for SMX degradation by UV is cleavage of S–N bond and C–S bond [7–67]. Consequently, a functional group of sulfones, an

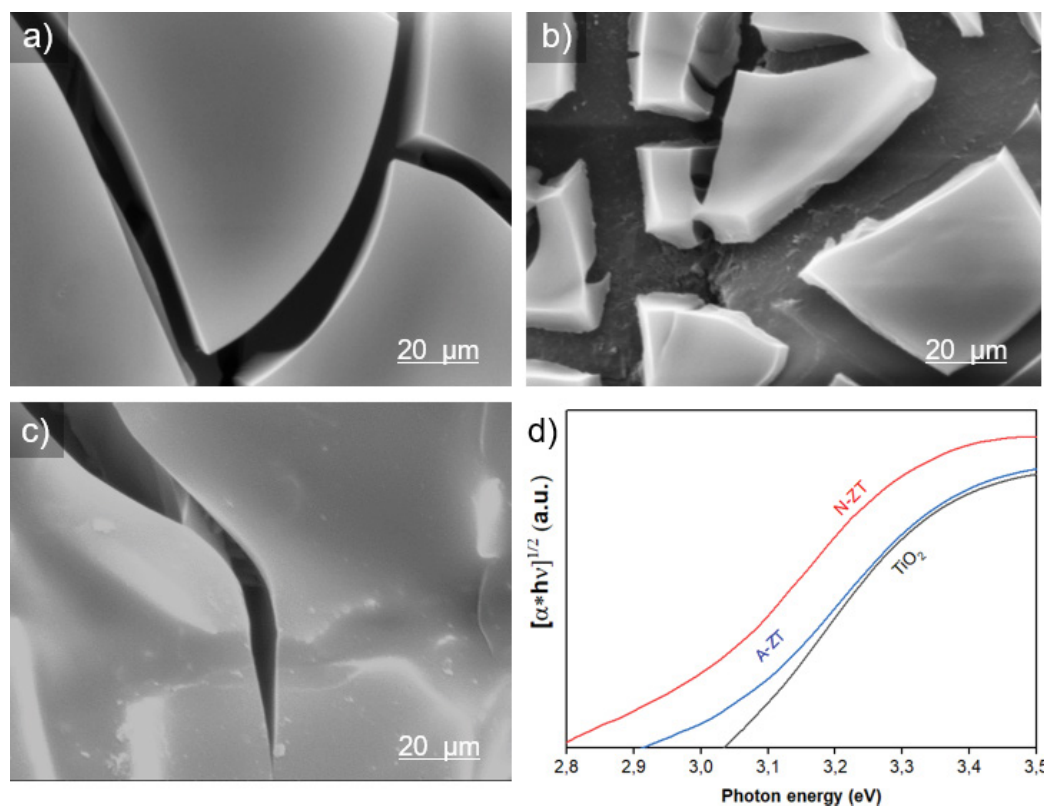


Fig. 3. MEV images of (a) TiO₂, (b) N-ZT and (c) A-ZT films, (d) optical band gap energy obtained from the Tauc method of catalysts.

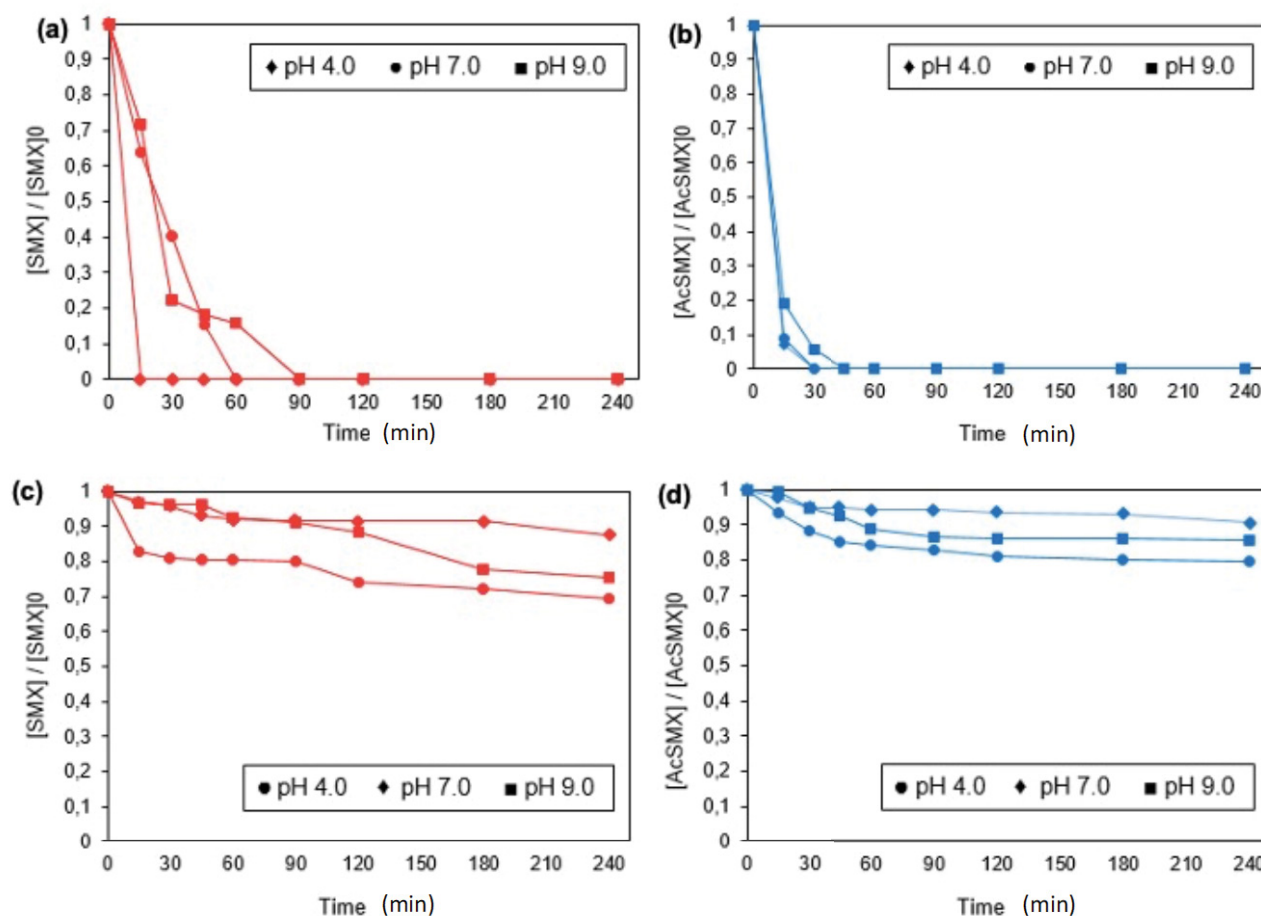


Fig. 4. Photolysis of SMX and AcSMX under UV-C (a, b) and UV-Vis (c, d) radiations at different pH. Initial concentration = 6 mg L⁻¹.

aniline ring and an isoxazole ring are formed. Several radicals produced during the photolysis of SMX cause the rearrangement of an isoxazole ring from the rupture of unstable N–O bond in an isoxazole ring.

Actinic lamp promoted 30.5%, 12.6% and 24.8% of SMX degradation at pH 4.0, 7.0 and 9.0, respectively. Actinic lamp has peaks of emission at 364, 404, 435, and 556 nm (Fig. S2). Even if SMX can not absorb visible radiation (>400 nm), it can absorb radiation at 364 nm. The highest SMX degradation efficiency was achieved at pH 4.0 (30.55%). According to Boreen et al. [68], SMX has greater light absorption and greater photochemical reactivity in its neutral form, leading to a shorter half-life time and higher decomposition efficiency. At pH 4.0, neutral SMX is the single dominant specie, considering by pK_a values (Table 1). Degradation of AcSMX was 20.52%, 9.42% and 14.31% at pH 4.0, 7.0 and 9.0, respectively.

On the other hand, when UV-C lamp was applied, AcSMX metabolite was completely degraded after 30 min at pH 4.0 and 7.0, and after 45 min at pH 9.0. At the same conditions, 100% of SMX degradation was also achieved. These results reaffirm the need to develop visible light active catalysts to degrade these compounds without the use of ultraviolet radiation.

3.3. Effects of operational parameters on photocatalysis

After preliminary photolysis tests, actinic lamp was chosen to evaluate the catalytic activity of the prepared materials. Effect of pH and target compound concentration were investigated.

3.3.1 Effect of pH

It is well known that pH changes not only influences molecule dissociation or surface charge of catalyst, but also the formation of [•]OH radicals in solution [69]. In this way, photocatalytic degradation would be greatly affected by pH value. This was confirmed by analyzing photocatalytic activity of immobilized catalysts at different pH values, which are presented in Fig. 5. The pH_{ZPC} of catalysts were determined and found to be about 7.0. The sulfamethoxazole is a diprotic molecule having dissociation constant values pK_{a1} and pK_{a2} of 1.85 and 5.6, respectively (Table 1). At pH 4.0 to 9.0, SMX species are in anionic form [66]. Indeed, at pH values lower than pH_{ZPC}, anionic SMX molecules tend to be adsorbed on the surface of the catalyst.

Concerning to TiO₂, SMX degradation was favored at pH 4.0, with maximum degradation efficiency of 57.6%. On the other hand, SMX showed an apparent degradation decrease

with the increase of pH solution. At pH 9.0, SMX degradation efficiency was 28.09% for TiO₂, the lowest compared to other catalysts. Increasing the pH caused an increase of negative charges sites on catalyst surface and more anionic SMX species formed, which perhaps favored in electrostatic repulsing of SMX molecule by the negatively charged TiO₂ surface [70,71].

According to Melo et al. [20], the lowest activity observed for A-ZT can be attributed to its pseudo-capacitive nature, that leads to charge accumulation on surface, resulting in high recombination rates. These properties will directly affect the redox capacity, thus lowering photocatalytic activity. In other hand, synergistic effect due to heterojunction was observed for N-ZT [20].

Huang et al. [72], described enhanced photocatalytic activity of Bi₂₅FeO₄₀/Cu₂O composite as a result of the efficient separation of photogenerated electrons and holes. Besides, SMX degradation efficiency of pure Cu₂O merely reached 45.8%, while for Bi₂₅FeO₄₀/Cu₂O composite 85% of SMX degradation was achieved. Liu et al. [73] evaluated SMX degradation with CeO₂/CN photocatalyst. The photodegradation efficiency of CeO₂/CN was higher than that for CN or CeO₂. In this regard, the better activity of N-ZT was attributed to the heterojunction. At pH 7.0, SMX degradation efficiency was 61.04% with N-ZT. At the same time, it was noted that at pH 4.0, lower efficiencies were achieved for N-ZT (47%) and A-ZT (38%) when compared to TiO₂ (58%). This substantial decrease of photocatalytic activity for ZnO based photocatalysts can be assigned to photocorrosion phenomenon occurring in acidic medium [74], thus compromising the stability of ZnO structures under UV radiation due to the self-oxidation [75]. Indeed, after atomic absorption analysis, the presence of Zn in the effluent treated at pH 4.00 was verified. Although the Zn concentration was very low (0.02 mg L⁻¹), close to the equipment error for a detection limit of 0.01–2.00 mg L⁻¹, this result is an indicative of photocorrosion of ZnO at acid pH. However, as showed in Fig. 4c, the concentration of compounds was hardly changed in the absence of photocatalyst. This clearly demonstrated that the thin N-ZT or A-ZT films possess characteristics that fairly enabled to enhance the degradation of sulfamethoxazole.

3.3.2 Effect of concentration

The effect of initial concentration on degradation rate in photocatalysis is shown in Fig. 6. A reduction in degradation efficiency was observed by increasing initial concentration from 2 to 6 and 10 mg L⁻¹, at constant pH of 7.0, using N-ZT thin film catalyst. Concentration increase caused a decrease on degradation of sulfamethoxazole from 58% (C₀ = 2 mg L⁻¹) to 49% (C₀ = 6 mg L⁻¹) and 36% (C₀ = 10 mg L⁻¹) for SMX, and from 42% to 32% and 20%, for AcSMX at initial concentrations of 2, 6 and 10 mg L⁻¹, respectively. This behavior can be assigned to the fact that the catalyst has more available superficial active sites at lower concentrations. Higher reactant concentration enhances the scavenging effect, causing a decrease in degradation efficiency [70]. Indeed, at higher concentrations, radiation becomes limiting, since azoxybenzene actinometry experiments proved that light is absorbed by the target compound as well as by the produced intermediates [71]. In addition, less active sites are available to be reached by photons and for adsorbing water or hydroxyl ions to proceed the generation of hydroxyl radicals by the catalyst.

3.4. Kinetics of photocatalytic degradation

The exponential decay observed in Fig. 6a and b suggests that the decomposition of SMX and AcSMX follows pseudo-first-order kinetics with acceptable R² values. In this sense, apparent first-order kinetics constants (*k*_{app}) at different initial concentrations of SMX and AcSMX were determined, and results are shown in Table 2, as well as half-life times and reaction rates. SMX concentration was reduced by 50% after 182 min and 248 min for initial concentration of 2 and 6 mg L⁻¹, respectively. Nevertheless, for high concentration such as 10 mg L⁻¹, more than 6 h of reaction were needed to reduce the concentration by 50%. For the metabolite, similar behavior was observed; however, more than 6 h of reaction would be needed to remove 50% of AcSMX at initial concentration of 2 mg L⁻¹. AcSMX proved to be quite resistant to photocatalytic degradation. Regardless of the initial concentration, the half-life time (*t*_{1/2}) was high

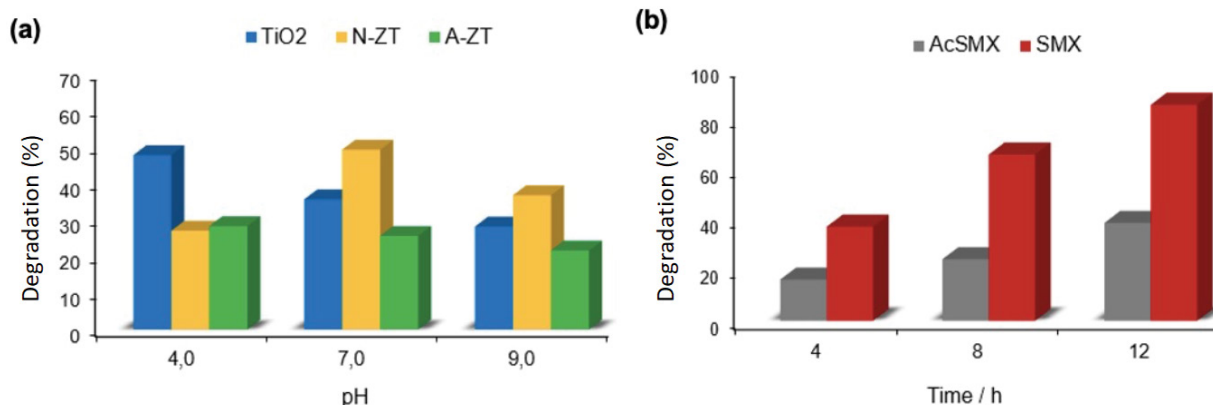


Fig. 5. Photocatalytic degradation under UV-Vis radiation (a) SMX at different pH value and (b) SMX or AcSMX using N-ZT as photocatalyst. Initial concentration = 6 mg L⁻¹, catalyst dose = 1.0 mg cm⁻².

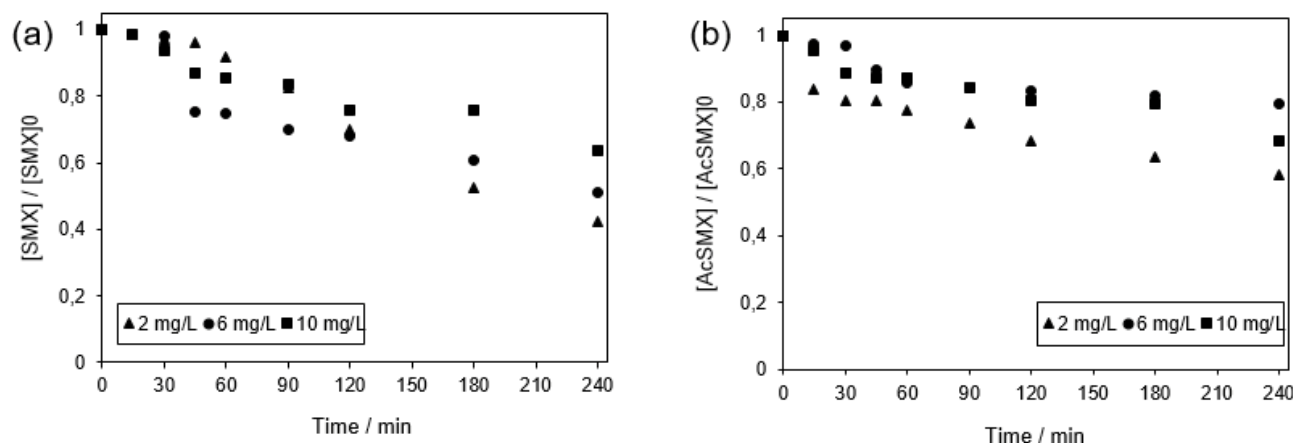


Fig. 6. Photocatalytic degradation using different initial (a) SMX or (b) AcSMX concentration over N-TZ under UV-Vis radiation. Catalyst dose = 1.0 mg cm^{-2} .

Table 2

Kinetic study of sulfamethoxazole and acetyl sulfamethoxazole (pH = 7.0 and N-TZ catalyst [1 mg cm^{-2}])

Concentration (mg L^{-1})	SMX				AcSMX			
	r_0 ($\text{mg L}^{-1} \text{ min}^{-1}$)	k_{app} (min^{-1})	R^2	$t_{1/2}$ (min)	r_0 ($\text{mg L}^{-1} \text{ min}^{-1}$)	k_{app} (min^{-1})	R^2	$t_{1/2}$ (min)
2	0.0076	0.0038	0.9726	182	0.0038	0.0019	0.9048	526
6	0.0168	0.0028	0.8962	248	0.0078	0.0013	0.9169	769
10	0.0180	0.0018	0.9430	385	0.0090	0.0009	0.7860	1111

when compared to SMX (Table 2). Other authors obtained for SMX k_{app} values of 0.0542 min^{-1} ($[\text{SMX}]_0 \sim 1.23 \text{ mg L}^{-1}$) with $\text{CoFe}_2\text{O}_4/\text{TiO}_2$ [76] and 0.0085 min^{-1} with $\text{Zn-TiO}_2/\text{biochar}$ ($[\text{SMX}]_0 = 10 \text{ mg L}^{-1}$) [77], proving that higher initial concentrations led to lower apparent reaction kinetics constants. It is worth to note that the variation on first-order kinetics constants with initial concentration occurs because its apparent value takes into account the intrinsic kinetics constant (which does not vary with concentration) and the adsorption rate, which varies with concentration of the reactant.

3.5. Evolution of photoproducts

The persistence of the degradation products was determined by running experiments for longer times (up to 12 h). These experiments were carried out with N-ZT photocatalyst at initial concentration of 6 mg L^{-1} for both SMX and AcSMX. After 12 h of reaction, 85.50% of SMX and 38.75% of AcSMX were degraded by photocatalytic process. This result confirms the higher resistance of metabolite AcSMX. Furthermore, the formation of by-products shown in Fig. 7a and b as seen in the chromatograms, photoproducts with similar retention times of SMX appeared in AcSMX photocatalysis. This means that metabolite molecule has been broken down and formed SMX compound in solution over again as reported in literature [7]. This result indicates that AcSMX metabolite can actually serve as precursor of SMX antibiotic into the environment and explain the lower degradation rates obtained for AcSMX, since photoproducts compete for photons, for adsorption

sites and oxidizing radicals in the medium. It can be verified by the reduction on intensity of SMX peak (indicated by *) when the chromatograms corresponding to 8 h and 12 h of irradiation are compared (Fig. 7a).

3.6. Photocatalytic mechanism

The carrier separation/transport mechanism in N-ZT heterostructures has been previously established [20]. When visible light irradiates N-ZT composite, charge carriers are photogenerated in both TiO_2 and ZnO-N (Fig. 8). Since the E_{CB} of TiO_2 was more negative than that of ZnO-N , the photogenerated electrons (e^-) of TiO_2 on the conduction band (CB) could be easily transferred to the conduction band of ZnO-N . Then, the photogenerated holes (h^+) on the valence band (VB) of ZnO-N could be injected into the valence band of TiO_2 since the E_{VC} of ZnO-N was more positive than that of TiO_2 . A facile charge carrier separation in the N-ZT composite enables hole accumulation to perform the oxidation of SMX and AcSMX. At the same time, the photogenerated electrons could reduce O_2 adsorbed in the solution to produce $\cdot\text{O}_2^-$ radicals. Furthermore, H_2O_2 and $\cdot\text{OH}$ radicals are generated, which further participation in the photocatalytic reaction.

Dlugosz et al. [78] proposed that the SMX molecule can undergo isomerization and hydroxylation reactions both in the aromatic ring and in the isoxazole ring, along with hydroxylation of the phenyl ring followed by cleavage of the N–O bond, leading to the formation of by-products. Additionally, hydrolysis and dimerization of SMX

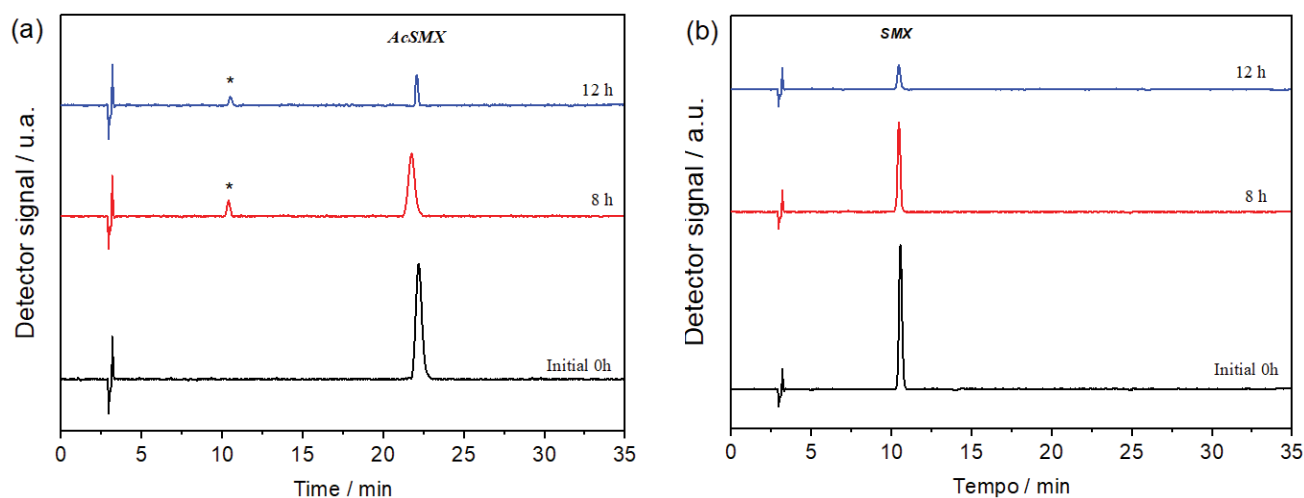


Fig. 7. Chromatograms showing the evolution of intermediates during degradation of 6 mg L^{-1} of (a) AcSMX and (b) SMX by photocatalytic reaction with 1.0 mg cm^{-2} of N-TZ.

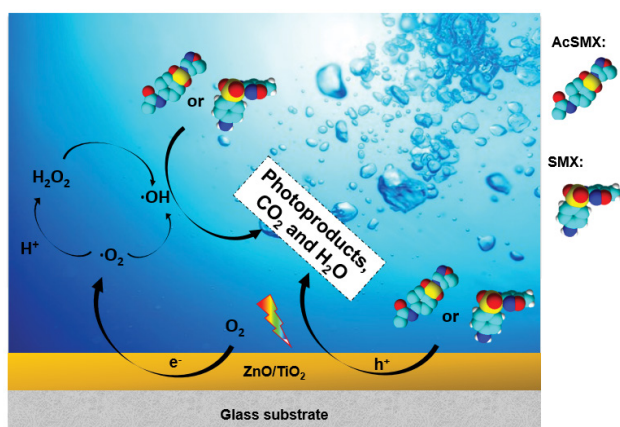


Fig. 8. Scheme of SMX and AcSMX degradation using N-TZ as photocatalyst.

by-products were also identified. Four hydroxylation products were identified, supporting the mechanism in which hydroxyl radicals are the active species.

3.7. Electrical energy consumption

The cost of treatment is one of the aspects that need more attention in advanced oxidative processes (AOP). Electrical energy per order (EE/O) was applied as a figure of merit in this study to evaluate and compare the degradation efficiency based on energy consumption according to Eq. (4). The results are shown in Table 3. EE/O for AcSMX photodegradation and photolysis were 1.6–2.9 times higher than that for SMX.

Operating costs of AOP treatment is highly dependent on the efficiency of a process. When UV-A radiation and TiO_2 were used by other authors, EE/O values of $21,060.2 \text{ kWh m}^{-3} \text{ order}^{-1}$ [78] and $52,115.3 \text{ kWh m}^{-3} \text{ order}^{-1}$ [79] for SMX degradation were found. The energy consumption required when immobilized N-ZT was applied

Table 3

EE/O values for photodegradation of sulfamethoxazole and metabolite over 4 h of reaction

Compound	EE/O ($\text{kWh m}^{-3} \text{ order}^{-1}$)	
	UV-Vis	UV-Vis/N-ZT
SMX	7,579	4,085
AcSMX	12,149	12,028

in this study is lower than that reported in other studies of photocatalytic degradation of SMX. The main reasons for the low energy consumption in this study could be the enhancement of degradation efficiency by heterojunction of TiO_2 and ZnO , which increased the efficiency of the photocatalyst. According to the best of our knowledge, EE/O values for AcSMX degradation by photolysis or photocatalysis has not been reported so far.

3.8. Residual toxicity assay

Cytotoxicity studies were carried out by applying *Lactuca sativa* seeds and *Artemia salina* as bioindicators and the results are presented in Fig. 9. The main toxic effect to *Lactuca sativa* seeds was the inhibition of root elongation, without inhibiting seed germination (Fig. 9a and b). As it can be seen in Fig. 9b, SMX was more phytotoxic than AcSMX. Although the photolysis of SMX under UV-C radiation proved to be more efficient on reducing the initial concentration, intermediates generated in this process proved to be more cytotoxic to *L. sativa* compared to UV-Vis photolysis and photocatalysis. Even though photocatalysis did not remove SMX with high efficiency, most SMX was transferred into low toxic intermediates which meant that residual toxicity was reduced.

Table 4 shows percent of live *A. salina* for different treatment conditions. Determination of the lethal dose for 50% of *A. salina* nauplii (LD_{50}) against SMX and AcSMX was

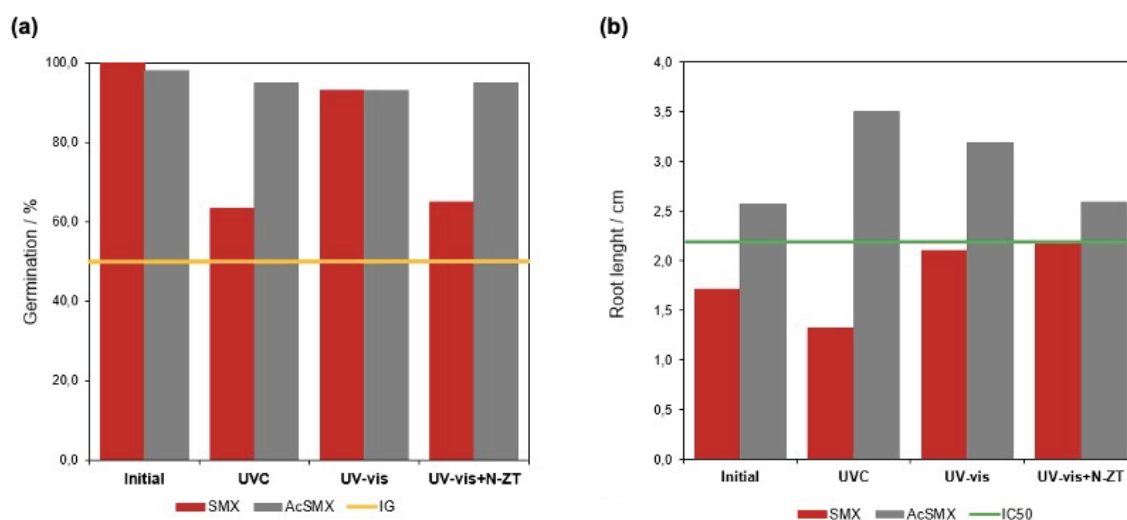


Fig. 9. Residual toxicity assay from *Lactuca sativa* (a) % of germination and (b) root length of initial and treated samples for photolytic and photocatalytic processes.

Table 4
Absolute (mean) percent of live *A. salina* for different treatment conditions

Samples		Percentage of effluent				
		15	35	50	75	100
SMX	Initial	100a*	100a	100a	60b	100a
	UV/Vis	100a	100a	100a	100a	100a
	UV/Vis + N-ZT	97a	100a	97a	87b	57c
AcSMX	Initial	97a	93a	87b	93a	90a
	UV/Vis	100a	100a	100a	100a	100a
	UV/Vis + N-ZT	93a	93a	97a	97a	100a

*Different letters mean statistically different values.

impossible to be performed since even the raw effluent did not kill half of the test population.

As it can be seen, for almost all the tests, there was no significant difference on *A. salina* lethality. At higher concentrations (75% and 100%), some photoproducts of photocatalytic degradation might be responsible for cytotoxicity against *A. salina* in the presence of catalyst. It is reported that SMX degradation can produce N-hydroxysulfamethoxazole (HO-SMX), known to be more recalcitrant than SMX and may be responsible for cytotoxicity [80,81]. At the same time, AcSMX photocatalytic degradation suggests that its residual toxicity was eliminated.

4. Conclusions

ZnO/TiO₂ heterostructured photocatalyst was successfully synthesized and characterized. The powder was immobilized on glass substrate and applied to the photodegradation of sulfamethoxazole (SMX) and its metabolite N-acetyl sulfamethoxazole (AcSMX). ZnO/TiO₂ was active under visible light, and about 49% and 32% of SMX and AcSMX degradation were observed after 240 min of

irradiation. Photocatalytic back-transformation of AcSMX to SMX was observed, indicating that this metabolite may serve as an environmental source of SMX antibiotic. The result underlines the importance to study this compound, since it is a metabolite originated by excretion, after consumption of the SMX antibiotic. Electrical energy required for antibiotic and metabolite degradation was determined, as well as toxic effect of treated samples. Some photoproducts generated by SMX photocatalytic degradation were responsible for cytotoxicity against *A. salina*. At the same time, photocatalytic degradation of AcSMX suggests that its initial toxicity was reduced.

Acknowledgement

The authors would like to thank the Brazilian agency CAPES for a PhD scholarship and the instrumental research facilities provided by the COMCAP/UEM.

References

- [1] A.J. van der Ven, T.B. Vree, E.W. van Ewijk-Beneken Kolmer, P.P. Koopmans, J.W. van der Meer, Urinary recovery and kinetics of sulphamethoxazole and its metabolites in HIV-seropositive patients and healthy volunteers after a single oral dose of sulphamethoxazole, *Br. J. Clin. Pharmacol.*, 39 (1995) 621–625.
- [2] N. Le-Minh, S.J. Khan, J.E. Drewes, R.M. Stuetz, Fate of antibiotics during municipal water recycling treatment processes, *Water Res.*, 44 (2010) 4295–4323.
- [3] F. Sopaj, N. Oturan, J. Pinson, F. Podvorica, M.A. Otura, Effect of the anode materials on the efficiency of the electro-Fenton process for the mineralization of the antibiotic sulfamethazine, *Appl. Catal., B*, 199 (2016) 331–341.
- [4] B. Kasprzyk-Hordern, R.M. Dinsdale, A.J. Guwy, The occurrence of pharmaceuticals, personal care products, endocrine disruptors and illicit drugs in surface water in South Wales, UK, *Water Res.*, 42 (2008) 3498–3518.
- [5] S. Willach, H.V. Lutze, K. Eckey, K. Löppenberg, M. Lülting, J.-B. Wolbert, D.M. Kujawinski, M.A. Jochmann, U. Karst, T.C. Schmidt, Direct photolysis of sulfamethoxazole using various irradiation sources and wavelength ranges—insights

- from degradation product analysis and compound-specific stable isotope analysis, *Environ. Sci. Technol.*, 52 (2018) 1225–1233.
- [6] X. Min, W. Li, Z. Wei, R. Spinney, D.D. Dionysiou, Y. Seo, C.J. Tang, Q. Li, R. Xiao, Sorption and biodegradation of pharmaceuticals in aerobic activated sludge system: a combined experimental and theoretical mechanistic study, *Chem. Eng. J.*, 342 (2018) 211–219.
- [7] F. Bonvin, J. Omlin, R. Rutler, W.B. Schweizer, P.J. Alaimo, T.J. Strathmann, K. McNeill, T. Kohn, Direct photolysis of human metabolites of the antibiotic sulfamethoxazole: evidence for abiotic back-transformation, *Environ. Sci. Technol.*, 47 (2013) 6746–6755.
- [8] C. Bouki, D. Venieri, E. Diamadopoulos, Detection and fate of antibiotic resistant bacteria in wastewater treatment plants: a review, *Ecotoxicol. Environ. Saf.*, 91 (2013) 1–9.
- [9] K. Noguera-Oviedo, D.S. Aga, Lessons learned from more than two decades of research on emerging contaminants in the environment, *J. Hazard. Mater.*, 316 (2016) 242–251.
- [10] P. Yan, Q. Sui, S. Lyu, H. Hao, H.F. Schröder, W. Gebhardt, Elucidation of the oxidation mechanisms and pathways of sulfamethoxazole degradation under Fe(II) activated percarbonate treatment, *Sci. Total Environ.*, 640–641 (2018) 973–980.
- [11] L. Gao, D. Minakata, Z. Wei, R. Spinney, D.D. Dionysiou, C.J. Tang, L. Chai, R. Xiao, Mechanistic study on the role of soluble microbial products in sulfate radical-mediated degradation of pharmaceuticals, *Environ. Sci. Technol.*, 53 (2019) 342–353.
- [12] A. Göbel, A. Thomsen, C.S. McArdell, A. Joss, W. Giger, Occurrence and sorption behavior of sulfonamides, macrolides, and trimethoprim in activated sludge treatment, *Environ. Sci. Technol.*, 39 (2005) 3981–3989.
- [13] M. Radke, C. Lauwigi, G. Heinkele, T.E. Mürdter, M. Letzel, Fate of the antibiotic sulfamethoxazole and its two major human metabolites in a water sediment test, *Environ. Sci. Technol.*, 43 (2009) 3135–3141.
- [14] K.L. Carstens, A.D. Gross, T.B. Moorman, J.R. Coats, Sorption and photodegradation processes govern distribution and fate of sulfamethazine in freshwater-sediment microcosms, *Environ. Sci. Technol.*, 47 (2013) 10877–10883.
- [15] J. Gou, Q. Ma, X. Deng, Y. Cui, H. Zhang, X. Cheng, X. Li, M. Xie, Q. Cheng, Fabrication of Ag_2O/TiO_2 -Zeolite composite and its enhanced solar light photocatalytic performance and mechanism for degradation of norfloxacin, *Chem. Eng. J.*, 308 (2017) 818–826.
- [16] J. Song, X. Wang, J. Ma, X. Wang, J. Wang, J. Zhao, Visible-light driven in situ inactivation of *Microcystis aeruginosa* with the use of floating g-C₃N₄ heterojunction photocatalyst: performance, mechanisms and implications, *Appl. Catal., B*, 226 (2018) 83–92.
- [17] M. Xing, J. Zhang, F. Chen, New approaches to prepare nitrogen-doped TiO₂ photocatalysts and study on their photocatalytic activities in visible light, *Appl. Catal., B*, 89 (2009) 563–569.
- [18] A. Hernández-Ramírez, I. Medina-Ramírez, *Photocatalytic Semiconductors: Synthesis, Characterization and Environmental Applications*, Springer, New York, 2015.
- [19] S. Bai, J. Jiang, Q. Zhang, Y. Xiong, Steering charge kinetics in photocatalysis: intersection of materials synthesis, characterization techniques and theoretical simulations, *Chem. Soc. Rev.*, 44 (2015) 2893–2939.
- [20] J.R. Melo, A.F. Gualdrón-Reyes, N.R.C. Fernandes, M.L. Gimenes, M.I. Carreño-Lizcano, I.N. Sequeda-Pico, J. Rodríguez-Pereira, V. Baldovino-Medrano, M.E. Niño-Gómez, How does the Zn-precursor nature impact carrier transfer in ZnO/Zn-TiO₂ nanostructures? Organic vs. inorganic anions, *New J. Chem.*, 43 (2019) 19085–19096.
- [21] M. Dahl, Y. Liu, Y. Yin, Composite titanium dioxide nanomaterials, *Chem. Rev.*, 114 (2014) 9853–9889.
- [22] S. Mukhopadhyay, P.P. Das, S. Maity, P. Ghosh, P.S. Devi, Solution grown ZnO rods: synthesis, characterization and defect mediated photocatalytic activity, *Appl. Catal., B*, 165 (2015) 128–138.
- [23] K.M. Lee, C.W. Lai, K.S. Ngai, J.C. Juan, Recent developments of zinc oxide based photocatalyst in water treatment technology: a review, *Water Res.*, 88 (2016) 428–448.
- [24] F.X. Xiao, S.F. Hung, H.B. Tao, J. Miao, H.B. Yang, B. Liu, Spatially branched hierarchical ZnO nanorod-TiO₂ nanotube array heterostructures for versatile photocatalytic and photoelectrocatalytic applications: towards intimate integration of 1D–1D hybrid nanostructures, *Nanoscale*, 24 (2014) 14950–14961.
- [25] M. Kwiatkowski, I. Bezverkhyya, M. Skompska, ZnO nanorods covered with a TiO₂ layer: simple sol-gel preparation, and optical, photocatalytic and photoelectrochemical properties, *Mater. Chem. A*, 3 (2015) 12748–12760.
- [26] M.R.D. Khaki, M.S. Shafeeyan, A.A.A. Raman, Wan M.A. Daud, Evaluating the efficiency of nano-sized Cu doped TiO₂/ZnO photocatalyst under visible light irradiation, *J. Mol. Liq.*, 258 (2018) 354–365.
- [27] S. Mukhopadhyay, D. Maiti, S. Chatterjee, P.S. Devi, G.S. Kumar, Design and application of Au decorated ZnO/TiO₂ as a stable photocatalyst for wide spectral coverage, *Phys. Chem. Chem. Phys.*, 18 (2016) 31622–31633.
- [28] M. Tobajas, C. Belver, J.J. Rodriguez, Degradation of emerging pollutants in water under solar irradiation using novel TiO₂-ZnO/clay nanoarchitectures, *Chem. Eng. J.*, 309 (2017) 596–606.
- [29] L.V. Cardoso, D. Tomasini, M.R.F. Sampaio, S.S. Caldas, N. Kleemann, E.G. Primel, F.F. Gonçalves, Optimization and validation of a method using SPE and LC-APCI-MS/MS for determination of pharmaceuticals in surface and public supply water, *J. Braz. Chem. Soc.*, 22 (2011) 1944–1952.
- [30] K. Lehnberg L. Kovalova, C. Kazner, T. Wintgens, T. Schettgen, T. Melin, J. Hollender, W. Dott., Degradation of Selected Organic Micropollutants from WWTP Effluent with Powdered Activated Carbon and Retention by Nanofiltration, Y.J. Kim, U. Platt, M.B. Gu, H. Iwahashi, Eds., *Atmospheric and Biological Environmental Monitoring*, Springer, Dordrecht, Heidelberg, New York, London, 2009, pp. 161–178.
- [31] S.O. Garcia, G.P. Pinto, P.A. Garcia-Encina, R.I. Mata, Ranking of concern, based on environmental indexes, for pharmaceutical and personal care products: an application to the Spanish case, *J. Environ. Manage.*, 129 (2013) 389–397.
- [32] R. Wahab, I.H. Hwang, Y.S. Kim, H.S. Shin, Photocatalytic activity of zinc oxide micro-flowers synthesized via solution method, *Chem. Eng. J.*, 168 (2011) 359–366.
- [33] M. Gusatti, D.A.R. Souza, N.C. Kuhnen, H.G. Riella, Growth of variable aspect ratio ZnO nanorods by solochemical processing, *J. Mater. Sci. Technol.*, 31 (2015) 10–15.
- [34] M.S.M. Ghazali, A. Zakaria, Z. Rizwan, H.M. Kamari, M. Hashim, M.H.M. Zaid, R. Zamiri, Use of a reflectance spectroscopy accessory for optical characterization of ZnO-BiO₂O₃-TiO₂ ceramics, *Int. J. Mol. Sci.*, 12 (2011) 1496–1504.
- [35] N. Ghobadi, Band gap determination using absorption spectrum fitting procedure, *Int. Nano Lett.*, 3 (2013) 2–4.
- [36] M. Meinert, G. Reiss, Electronic structure and optical band gap determination of NiFe₂O₄, *J. Phys.: Condens. Matter*, 26 (2014) 1–4.
- [37] S. Jorfi, G. Barzegar, M. Ahmadi, R.D.C. Soltanid, N.J. Haghhighifard, A. Takdastan, R. Saeedi, M. Abtahi, Enhanced coagulation-photocatalytic treatment of Acid red 73 dye and real textile wastewater using UVA/synthesized MgO nanoparticles, *J. Environ. Manage.*, 177 (2016) 111–118.
- [38] J.R. Bolton, K.G. Bircher, W. Tumas, C.A. Tolman, Figures of merit for the technical development and application of advanced oxidation processes, *J. Adv. Oxid. Technol.*, 1 (1996) 13–17.
- [39] J.C. Garcia, T.K.F.S. Freitas, S.M. Palácio, E. Ambrósio, M.T.F. Souza, Toxicity assessment of textile effluents treated by advanced oxidative process (UV/TiO₂ and UV/TiO₂/H₂O₂) in the species *Artemia salina* L., *Environ. Monit. Assess.*, 185 (2013) 2179–2187.
- [40] M.C. Ortega, M.T. Moreno, J. Ordovás, M.T. Aguado, Behaviour of different horticultural species in phytotoxicity bioassays of bark substrates, *Sci. Hortic.*, 66 (1996) 125–132.

- [41] United States Environmental Protection Agency (USEPA), Ecological Effects Test Guidelines OPPTS 850.4200 – Seed germination/Root Elongation Toxicity Test. P.a. T. S. Prevention, Washington D.C., 1996.
- [42] T. Giannakopoulou, N. Todorova, M. Giannouri, J. Yu, C. Trapalis, Optical and photocatalytic properties of composite TiO₂/ZnO thin films, *Catal. Today*, 230 (2014) 174–180.
- [43] R. Liu, H. Ye, X. Xiong, H. Liu, Fabrication of TiO₂/ZnO composite nanofibers by electrospinning and their photocatalytic property, *Mater. Chem. Phys.*, 121 (2010) 432–439.
- [44] M. Pérez-González, S.A. Tomás, M. Morales-Luna, M.A. Arvizu, M.M. Tellez-Cruz, Optical, structural, and morphological properties of photocatalytic TiO₂-ZnO thin films synthesized by the sol-gel process, *Thin Solid Films*, 594 (2015) 304–309.
- [45] M. Zalfani, B.V. Schueren, M. Mahdouan, R. Bourguiga, W.B. Yu, M. Wu, O. Deparis, Y. Li, B.L. Su, ZnO quantum dots decorated 3DOM TiO₂ nanocomposites: symbiose of quantum size effects and photonic structure for highly enhanced photocatalytic degradation of organic pollutants, *Appl. Catal., B*, 199 (2016) 187–198.
- [46] A. Pérez-Larios, R. Lopez, A. Hernández-Gordillo, F. Tzompantzia, R. Gómez, L.M. Torres-Guerra, Improved hydrogen production from water splitting using TiO₂-ZnO mixed oxides photocatalysts, *Fuel*, 100 (2012) 139–143.
- [47] Y. Chen, C. Zhang, W. Huang, C. Yang, T. Huang, Y. Situ, H. Huang, Synthesis of porous ZnO/TiO₂ thin films with superhydrophilicity and photocatalytic activity via a template-free sol-gel method, *Surf. Coat. Technol.*, 258 (2014) 531–538.
- [48] O. Frank, M. Zukalova, B. Laskova, J. Kürti, J. Koltaib, L. Kavan, Raman spectra of titanium dioxide (anatase, rutile) with identified oxygen isotopes (16, 17, 18), *Phys. Chem. Chem. Phys.*, 14 (2012) 14567–14572.
- [49] L. Miao, S. Tanemura, S. Toh, K. Kaneko, M. Tanemura, Fabrication, characterization and Raman study of anatase-TiO₂ nanorods by a heating-sol-gel template process, *J. Cryst. Growth*, 264 (2004) 246–252.
- [50] F. Tian, Y. Zhang, J. Zhang, C. Pan, Raman spectroscopy: a new approach to measure the percentage of anatase TiO₂ exposed (001) facets, *J. Phys. Chem. C*, 116 (2012) 7515–7519.
- [51] Z.W. Dong, C.F. Zhang, H. Deng, G.J. You, S.X. Qian, Raman spectra of single micrometer-sized tubular ZnO, *Mater. Chem. Phys.*, 99 (2006) 160–163.
- [52] N.P. Herring, L.S. Panchakarla, M.S. El-Shall, P-Type nitrogen-doped ZnO nanostructures with controlled shape and doping level by facile microwave synthesis, *Langmuir*, 30 (2014) 2230–2240.
- [53] N. Naseria, M. Yousefi, A.Z. Moshfegh, A comparative study on photoelectrochemical activity of ZnO/TiO₂ and TiO₂/ZnO nanolayer systems under visible irradiation, *Solar Energy*, 85 (2011) 1972–1978.
- [54] M.M. Karkare, Choice of precursor not affecting the size of anatase TiO₂ nanoparticles but affecting morphology under broader view, *Int. Nano Lett.*, 4 (2014) 111, doi: 10.1007/s40089-014-0111-x.
- [55] H. Khan, D. Berk, Effect of a chelating agent on the physicochemical properties of TiO₂: characterization and photocatalytic activity, *Catal. Lett.*, 144 (2014) 890–904.
- [56] D. Tsiourvas, A. Tsetsekou, M. Arkas, S. Diplas, E. Mastrogrianni, Covalent attachment of a bioactive hyperbranched polymeric layer to titanium surface for the biomimetic growth of calcium phosphates, *J. Mater. Sci.: Mater. Med.*, 22 (2011) 85–96.
- [57] K. Zak, W.H. Abd. Majid, M.R. Mahmoudian, M. Darroudi, R. Yousefi, Starch-stabilized synthesis of ZnO nanopowders at low temperature and optical properties study, *Adv. Powder Technol.*, 24 (2013) 618–624.
- [58] F. Gualdrón-Reyes, A.M. Meléndez, I. González, L. Lartundo-Rojas, M.E. Niño-Gómez, Effect of metal substrate on photo(electro)catalytic activity of B-doped graphene modified TiO₂ thin films: role of iron oxide nanoparticles at grain boundaries of TiO₂, *Phys. Chem. C*, 122 (2018) 297–306.
- [59] M.I. Carreño-Lizcano, A.F. Gualdrón-Reyes, V. Rodríguez-González, J.A. Pedraza-Avella, M.E. Niño-Gómez, Photoelectrocatalytic phenol oxidation employing nitrogen doped TiO₂-rGO films as photoanodes, *Catal. Today*, 341 (2020) 96–103.
- [60] D. Sethi, R. Sakthivel, ZnO/TiO₂ composites for photocatalytic inactivation of Escherichia coli, *J. Photochem. Photobiol., B*, 168 (2017) 117–123.
- [61] L.J. Hoyos, D.F. Rivera, A.F. Gualdrón-Reyes, R. Ospina, J. Rodríguez-Pereira, J.L. Roperro-Veja, M.E. Niño-Gómez, Influence of immersion cycles during n-β-Bi₂O₃ sensitization on the photoelectrochemical behaviour of N-F co-doped TiO₂ nanotube, *Appl. Surf. Sci.*, 423 (2017) 917–926.
- [62] D. Ramírez-Ortega, P. Acevedo-Peña, F. Tzompantzi, R. Arroyo, F. González, I. González, Energetic states in SnO₂-TiO₂ structures and their impact on interfacial charge transfer process, *J. Mater. Sci.*, 52 (2017) 260–275.
- [63] T.H. Kim, S.D. Kim, H.Y. Kim, S.J. Lim, M. Lee, S. Yu, Degradation and toxicity assessment of sulfamethoxazole and chlortetracycline using electron beam, ozone and UV, *J. Hazard. Mater.*, 227–228 (2012) 237–242.
- [64] S. Luo, Z. Wei, R. Spinney, Z. Zhang, D.D. Dionysiou, L. Gao, L. Chai, D. Wang, R. Xiao, UV direct photolysis of sulfamethoxazole and ibuprofen: an experimental and modeling study, *J. Hazard. Mater.*, 343 (2018) 132–139.
- [65] G. Trovó, R.F.P. Nogueira, A. Agüera, C. Sirtori, A.R. Fernández-Alba, Photodegradation of sulfamethoxazole in various aqueous media: persistence, toxicity and photoproducts assessment, *Chemosphere*, 77 (2009) 1292–1298.
- [66] L. Boreen, W.A. Arnold, K. McNeill, Photochemical fate of sulfa drugs in the aquatic environment: sulfa drugs containing five-membered heterocyclic groups, *Environ. Sci. Technol.*, 38 (2004) 3933–3940.
- [67] J. Zhang, Y. Nosaka, Mechanism of the radical OH generation in photocatalysis with TiO₂ of different Crystalline types, *J. Phys. Chem.*, 118 (2014) 10824–10832.
- [68] A. Tiwari, A. Shukla, Lalliansanga, D. Tiwari, S.M. Lee, Nanocomposite thin films Ag⁰(NP)/TiO₂ in the efficient degradation of micropollutants from aqueous solutions: a case study of tetracycline and sulfamethoxazole degradation, *J. Environ. Manage.*, 220 (2018) 96–108.
- [69] D. Nasuhoglu, V. Yargeau, D. Berk, Photo-degradation of sulfamethoxazole (SMX) by photolytic and photocatalytic processes in a batch reactor under UV-C radiation (λ_{max} = 254 nm), *J. Hazard. Mater.*, 186 (2011) 67–75.
- [70] H. Gong, W. Chu, Photodegradation of sulfamethoxazole with a recyclable catalyst, *Ind. Eng. Chem. Res.*, 54 (2015) 12763–12769.
- [71] X. Xie, S. Li, H. Zhang, Z. Wang, H. Huang, Promoting charge separation of biochar-based Zn-TiO₂/pBC in the presence of ZnO for efficient sulfamethoxazole photodegradation under visible light irradiation, *Sci. Total Environ.*, 659 (2019) 529–539.
- [72] Y. Huang, L. Nengzi, X. Li, L. Meng, Q. Song, X. Cheng, Fabrication of Cu₂O/Bi₂FeO₄ nanocomposite and its enhanced photocatalytic mechanism and degradation pathways of sulfamethoxazole, *Mater. Sci. Semicond. Process.*, 109 (2020) 104932, doi: 10.1016/j.mssp.2020.104932.
- [73] G. Liu, H. Wang, D. Chen, C. Dai, Z. Zhang, Y. Feng, Photodegradation performances and transformation mechanism of sulfamethoxazole with CeO₂/CN heterojunction as photocatalyst, *Sep. Purif. Technol.*, 237 (2020) 116329, doi: 10.1016/j.seppur.2019.116329.
- [74] M. Shirzad-Siboni, A. Khataee, B. Vahid, S.W. Joo, Synthesis, Characterization and immobilization of ZnO nanosheets on scallop shell for photocatalytic degradation of an insecticide, *Sci. Adv. Mater.*, 7 (2015) 806–814.
- [75] F. Yuan, C. Hu, X. Hu, J. Qu, M. Yang, Degradation of selected pharmaceuticals in aqueous solution with UV and UV/H₂O₂, *Water Res.*, 43 (2009) 1766–1774.
- [76] M. Valery, N. Mouamfon, W. Li, S. Lu, N. Chen, Z. Qiu, K. Lin, Photodegradation of sulfamethoxazole applying UV- and VUV-based processes, *Water Air Soil Pollut.*, 218 (2011) 265–274.
- [77] J.C. Carlson, M.I. Stefan, J.M. Parnis, C.D. Metcalfe, Direct UV photolysis of selected pharmaceuticals, personal care products and endocrine disruptors in aqueous solution, *Water Res.*, 84 (2015) 350–361.

- [78] M. Długosz, P. Żmudzki, A. Kwiecień, K. Szczubiałka, J. Krzek, M. Nowakowska, Photocatalytic degradation of sulfamethoxazole in aqueous solution using a floating TiO_2 -expanded perlite photocatalyst, *J. Hazard. Mater.*, 298 (2015) 146–153.
- [79] C. Yang, C.L. Huang, T.C. Cheng, H.T. Lai, Inhibitory effect of salinity on the photocatalytic degradation of three sulfonamide antibiotics, *Int. Biodeterior. Biodegrad.*, 102 (2015) 116–125.
- [80] Y.B. Zhang, J. Zhou, Q.M. Xu, J.S. Cheng, Y.L. Luo, Y.J. Yuan, Exogenous cofactors for the improvements of sulfamethoxazole (SMX) biodegradation and biotransformation by *Alcaligenes faecalis*, *Sci. Total Environ.*, 565 (2016) 547–556.
- [81] X. Li, Q.M. Xu, J.S. Cheng, Y.J. Yuan, Improving the biodegradation of sulfamethoxazole and alleviating cytotoxicity of its biotransformation by laccase producing system under coculture of *Pycnoporus sanguineus* and *Alcaligenes faecalis*, *Bioresour. Technol.*, 220 (2016) 333–340.

Supplementary information

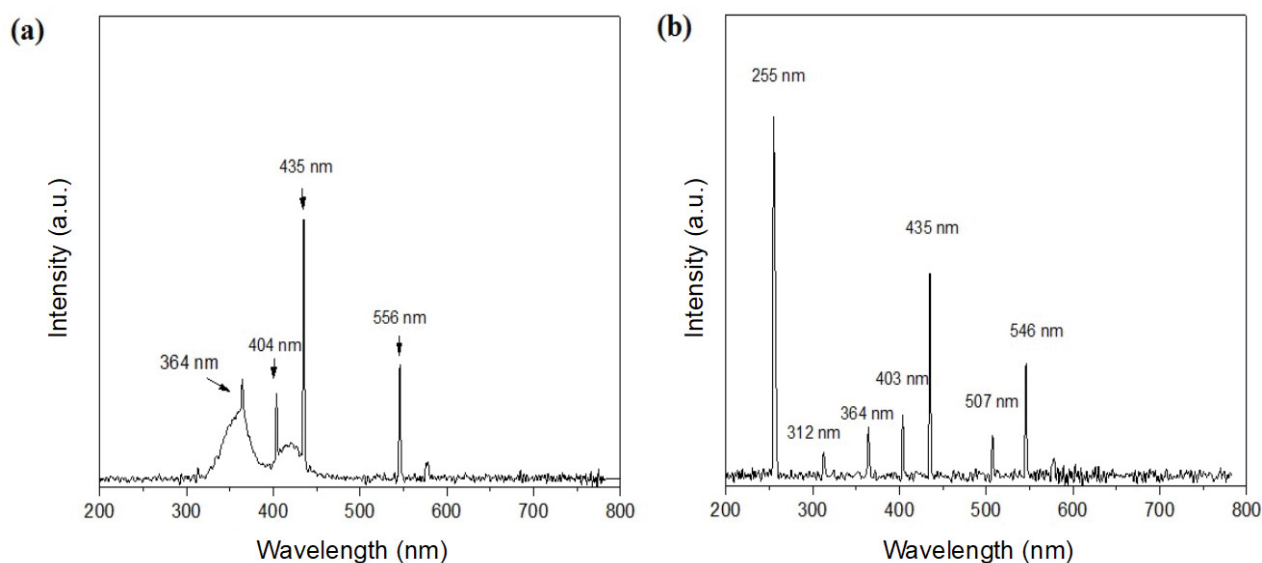


Fig. S1. Emission spectra of the lamps: (a) actinic (LUCMAT) and (b) germicide (OSRAM).

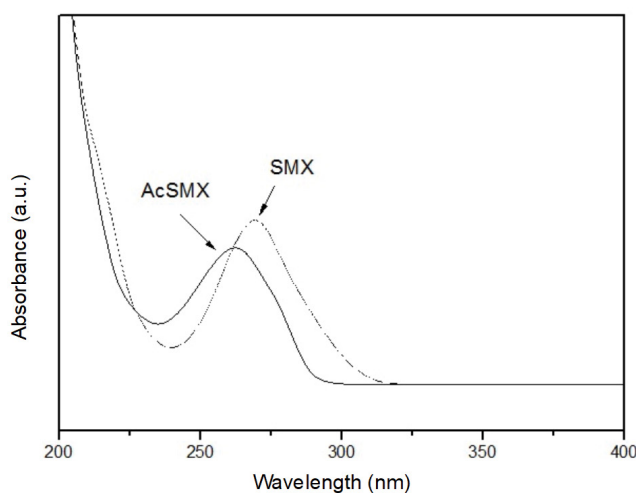


Fig. S2. SMX and AcSMX UV-Vis absorption spectra at 6.00 mg L^{-1} and $\text{pH} = 7.00$.